


**Observations of active galaxies with
high spatial resolution with
Kyoto tridimensional spectrograph II**

H. Sugai, A. Kawai, T. Hattori, S. Ozaki,
G. Kosugi, A. Shimono, H. Ohtani, T. Hayashi,
T. Ishigaki, M. Ishii, M. Sasaki

What is Kyoto 3DII???

Answer: **PI instrument** of Subaru

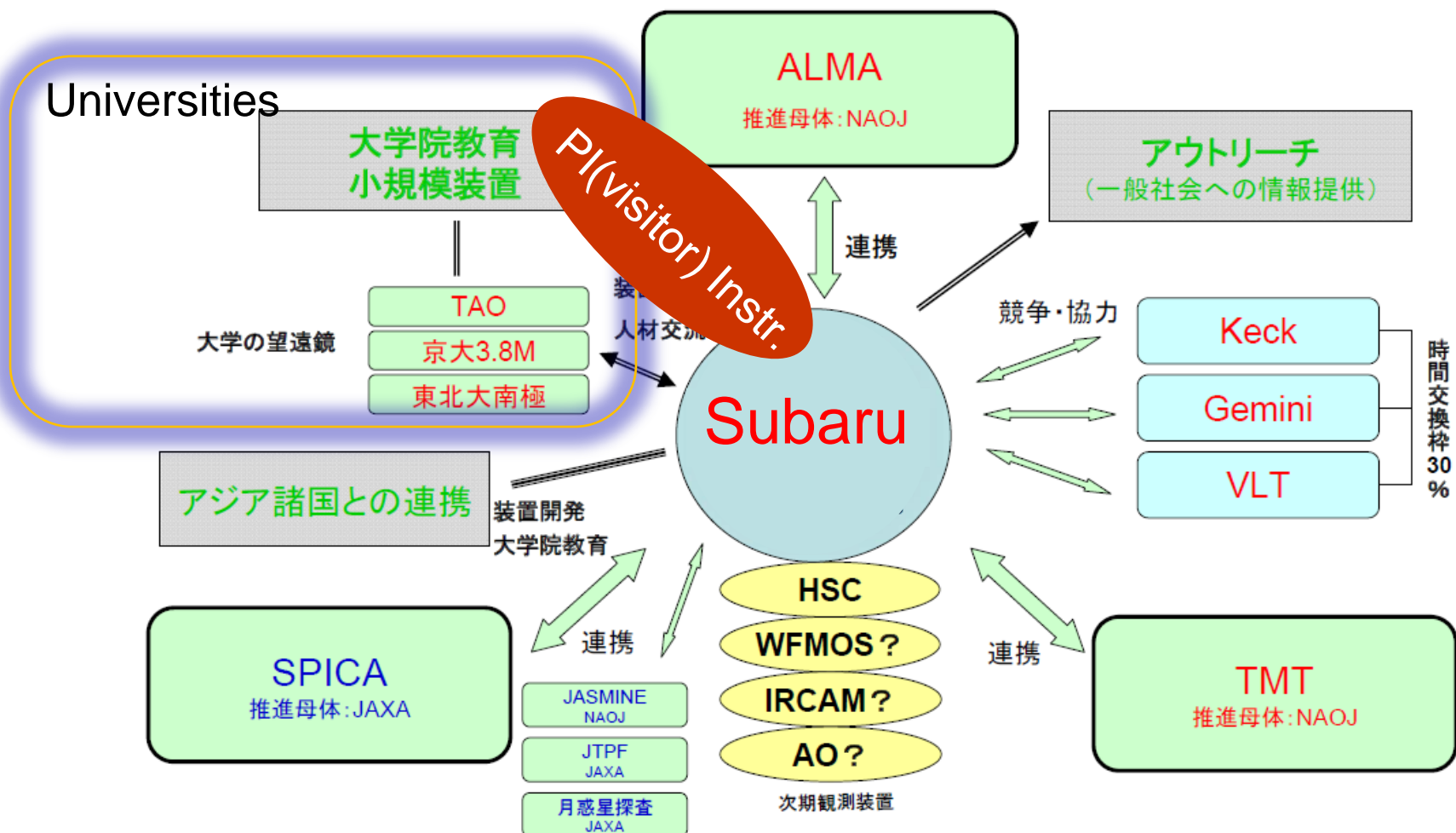
PI instruments	If you want to use the PI instruments such as CIAO or Kyoto3DII, please make contact with the instrument team in advance. The contact address for CIAO is <i>ishii@naoj.org</i> , and for Kyoto3DII is <i>sugai@kusastro.kyoto-u.ac.jp</i>
---------------------------	--



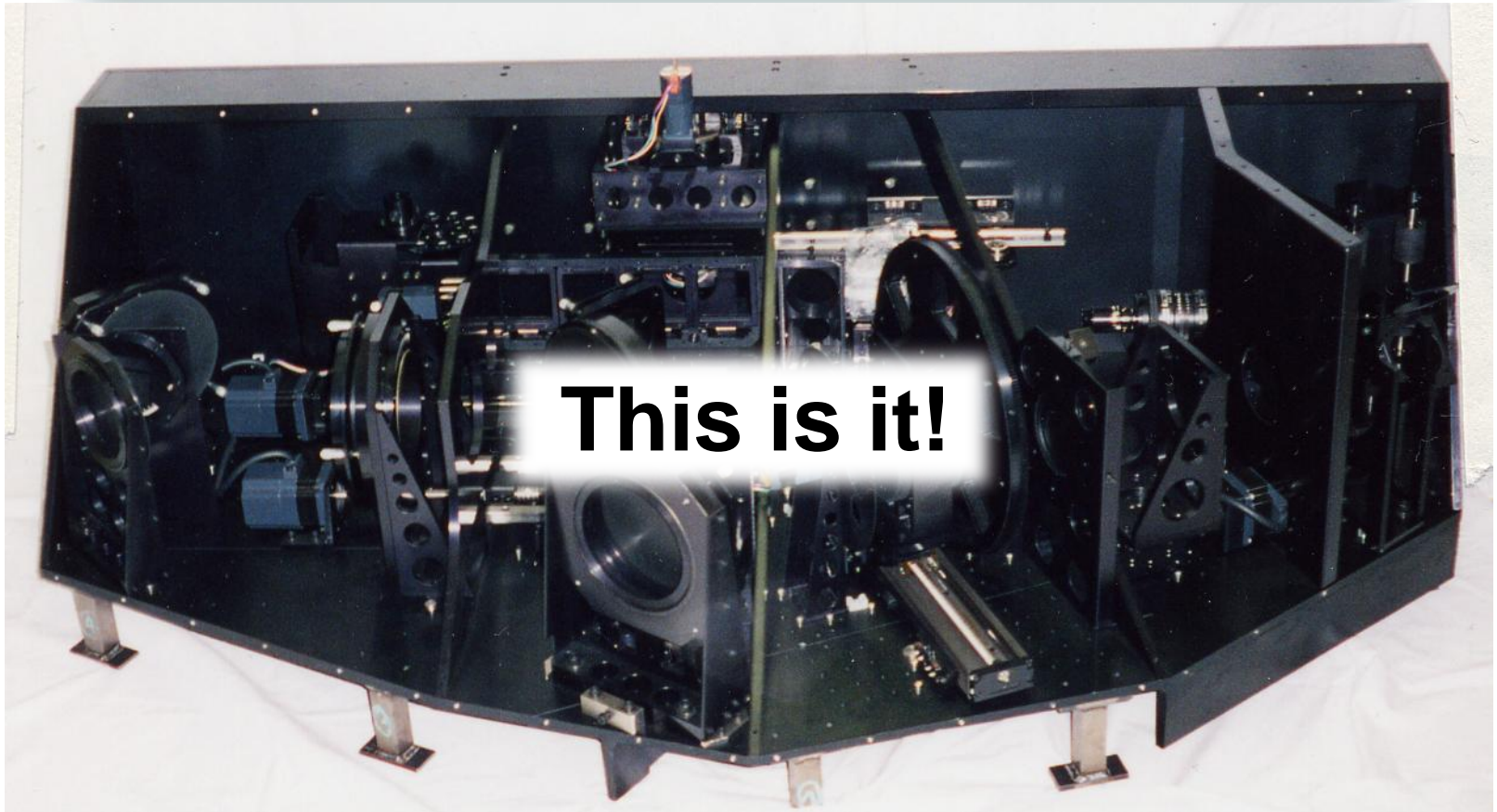
<http://subarutelescope.org/Observing/Proposals/Submit/call.html>

Proposals from Subaru Advisory Committee to NAOJ Opt/IR Technical Committee

光赤外専門委員会への提言案
 --2020年へのすばるの戦略 “天・地・人”-- 2008.10.16
 すばる小委員会



What is Kyoto 3DII??



1.5m



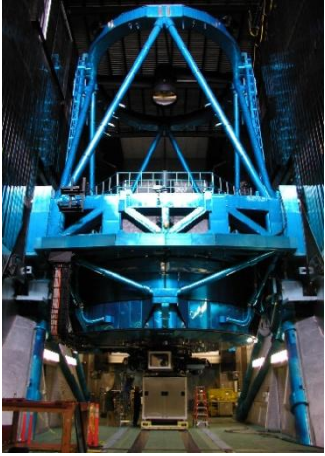
150kg

What is Kyoto 3DII?

Multi-mode Optical (**360-900nm**) Spectrograph
at Cassegrain

- i) Lenslet-type Integral Field Spectrograph (IFS)
- ii) Fabry-Perot
- iii) Slit Spectrograph
- iv) Filter Imaging

(test observations on 1.5m tel in Tokyo before those at Mauna Kea)
cf. Nasmyth focus in case of 3DII + AO188



on Subaru Cass.
(2002 Aug)

Table 1: Observing Parameters

Observational mode	On Subaru (8.2 m, F/12.2)
Fabry-Perot	$0''.056 \text{ pixel}^{-1}$ ^a Field of view $1'.9 \times 1'.9$ (Velocity shift $\Delta v \text{ (km s}^{-1}\text{)} = 980 \times (\theta')^2$ $R \equiv \lambda/\Delta\lambda \sim 400 \text{ and } 7000$ $(400 - 700 \text{ nm})$ ^c
Integral field spectrograph with a lenslet array (+ 34× enlarger)	$0''.096 \text{ lens}^{-1}$ Field of view $3''.6 \times 2''.8(\text{object}) + 3''.6 \times 0''.6(\text{sky})$ $R \simeq 1200 \text{ (360 - 900 nm)}$ ^{d,e}
Long slit	Width $0''.12, 0''.19, 0''.56$ or Width $0''.17, 0''.62, 2''.1$ Length $1'.5$ $R \simeq 1200 \text{ for } 0''.12 \text{ slit}$ ^d
Narrow-band imaging	$0''.056 \text{ pixel}^{-1}$ Field of view $1'.9 \times 1'.9$

Kyoto 3DII Presentations in this conference

1. Observations of active galaxies with high spatial resolution with Kyoto tridimensional spectrograph II
--- Sugai et al., this talk
2. M87 Nucleus Observed with the **Integral Field Spectrograph** Mode of Kyoto3DII
--- Nakajima et al. (B-5)
3. Galactic Wind in the Nearby Starburst Galaxy NGC 253 Observed with the Kyoto3DII **Fabry-Perot** Mode
--- Matsubayashi et al. (E-9)
4. Integrating Kyoto3DII with Subaru/**AO188** for improved image-quality observation in optical
--- Shimono et al. (F-6)

Examples of high resolution observations

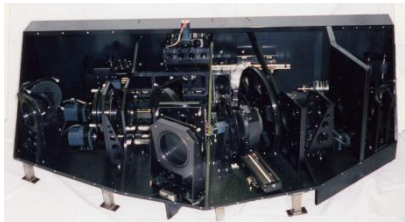
1. “Subarcsecond structure and velocity field of optical line-emitting gas in NGC 1052”

H. Sugai, T. Hattori, A. Kawai, S. Ozaki, G. Kosugi, H. Ohtani,
T. Hayashi, T. Ishigaki, M. Ishii, M. Sasaki, N. Takeyama,
M. Yutani, T. Usuda, S. S. Hayashi, K. Namikawa, 2005, ApJ, 629, 131.

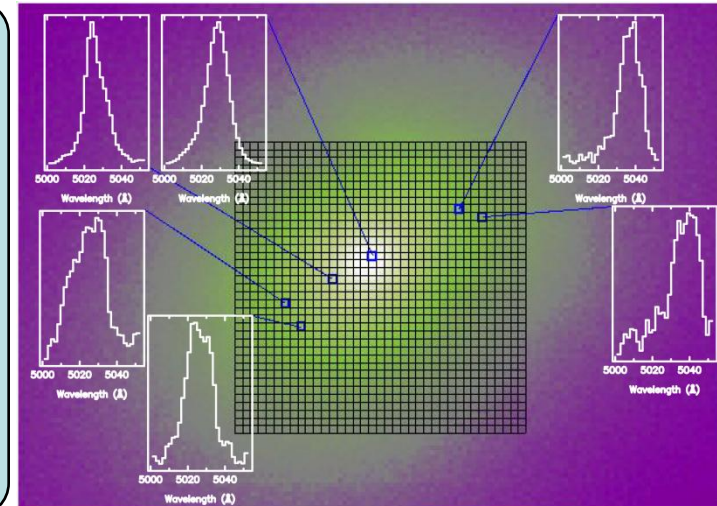
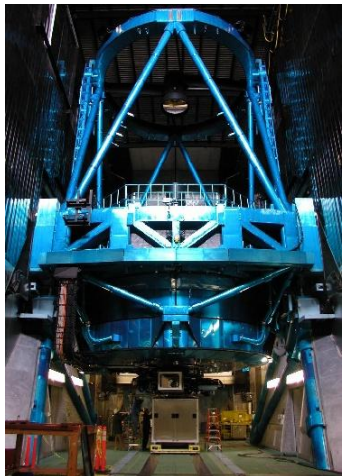
2. “Integral field spectroscopy of the quadruply lensed quasar 1RXS J1131-1231: new light on lens substructures”

H. Sugai, A. Kawai, A. Shimono, T. Hattori, G. Kosugi,
N. Kashikawa, K. T. Inoue, M. Chiba, 2007, ApJ, 660, 1016.

Subarcsecond structure and velocity field of optical line-emitting gas in NGC 1052



1. Background
2. Abstract
3. Observations
4. Results
 - 4-1. Three components
 - 4-2. Structures in bipolar outflow
 - 4-3. Bipolar outflow & radio jets
5. Summary



Background: LINER studies

Studies of LINERs (Low Ionization Nuclear Emission-line Regions)

Heckman (1980)

---activity clearly distinct from those of starbursts and of classical AGNs

Ho et al. (1997,1996)

---in over 30% of all galaxies (in 60% of Sa-Sab) with $B < 12.5$ mag

Discussion on Ionization/excitation mechanisms

(e.g., Sugai & Malkan 2000; Gabel et al. 2000; Kadler et al. 2004;

Ho et al. 2001; Eracleous et al. 2002; Terashima & Wilson 2003)

- sizes are **small**. a few to several arcseconds.
 - **complex and disordered** morphologies
(HST filter imaging: Pogge et al. 2000)
- 3DII on Subaru --- resolving these faint and small objects in data cube

Background: NGC 1052

- pure **AGN outflow**

complication for AGN-driven outflows: they sometimes coexist with starburst-driven winds (Veilleux et al. 2005)

---no evidence of starbursts in NGC 1052

- **young** activities

similar to Gigahertz-Peaked-Spectrum or Compact-Steep-Spectrum sources

the entire radio source contained within the host galaxy.
a convex radio spectrum peaked at 10 GHz.

-> young jets, propagating through, and perhaps interacting with, a rich inner galactic medium

Abstract (NGC 1052)

Three main components:

(1) low velocity disk rotation

(2) high velocity bipolar **outflow**

outflow axis does not coincide with disk rotation axis.

(3) spatially unresolved nuclear component

Outflow structure:

opening angle decreases with velocity shift from the systemic velocity both in bluer and redder velocity channels.

-> **intrinsically higher-velocity components inside.**

highest velocity components are detached from the nucleus.

-> **acceleration?**

bow shocks by even higher velocity (unseen) outflow components?

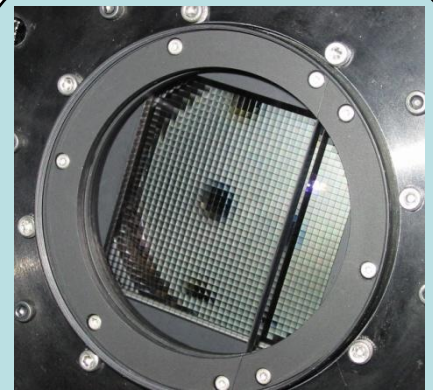
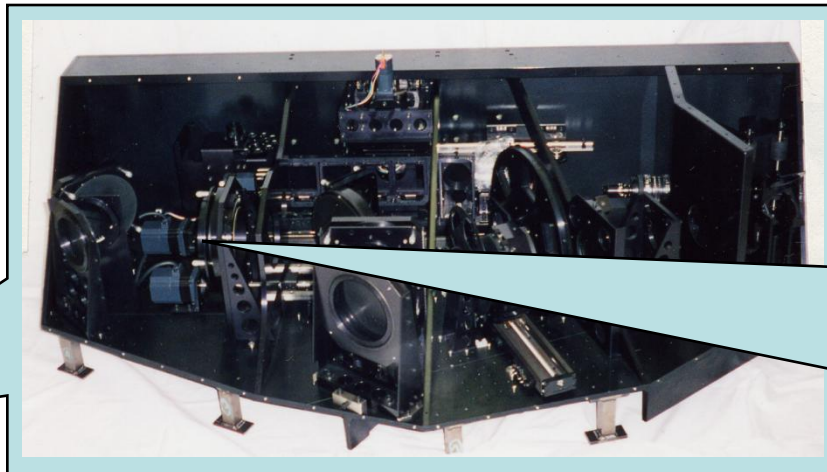
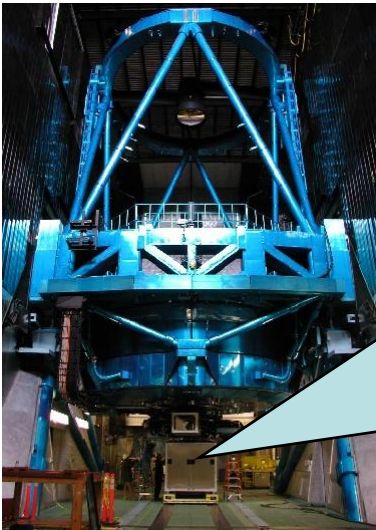
Strong [OIII] emission **ridges**

-> closely **related to 1"-scale radio jet-counterjet structure.**

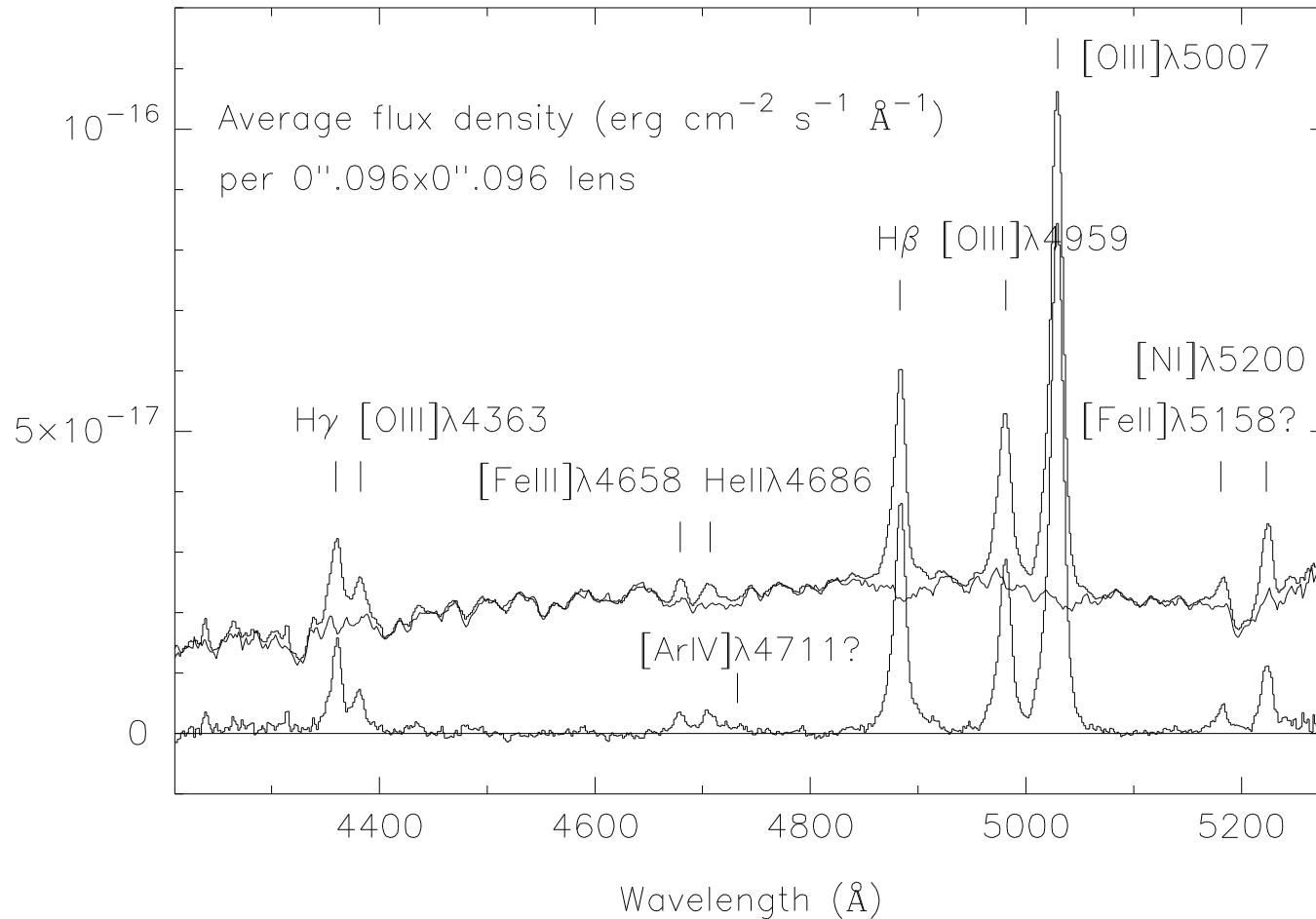
Observations

Kyoto 3DII **IFS** mode (37x37 lenslet array)
+ Subaru 8.2m telescope

- 4200-5200Å (a 60min exposure, $R=1200$)
- Spatial sampling = $0''.096 \text{ lenslet}^{-1}$
→ Field of View $\sim 3''.6 \times 2''.8$
- Spatial resolution = $0''.4$

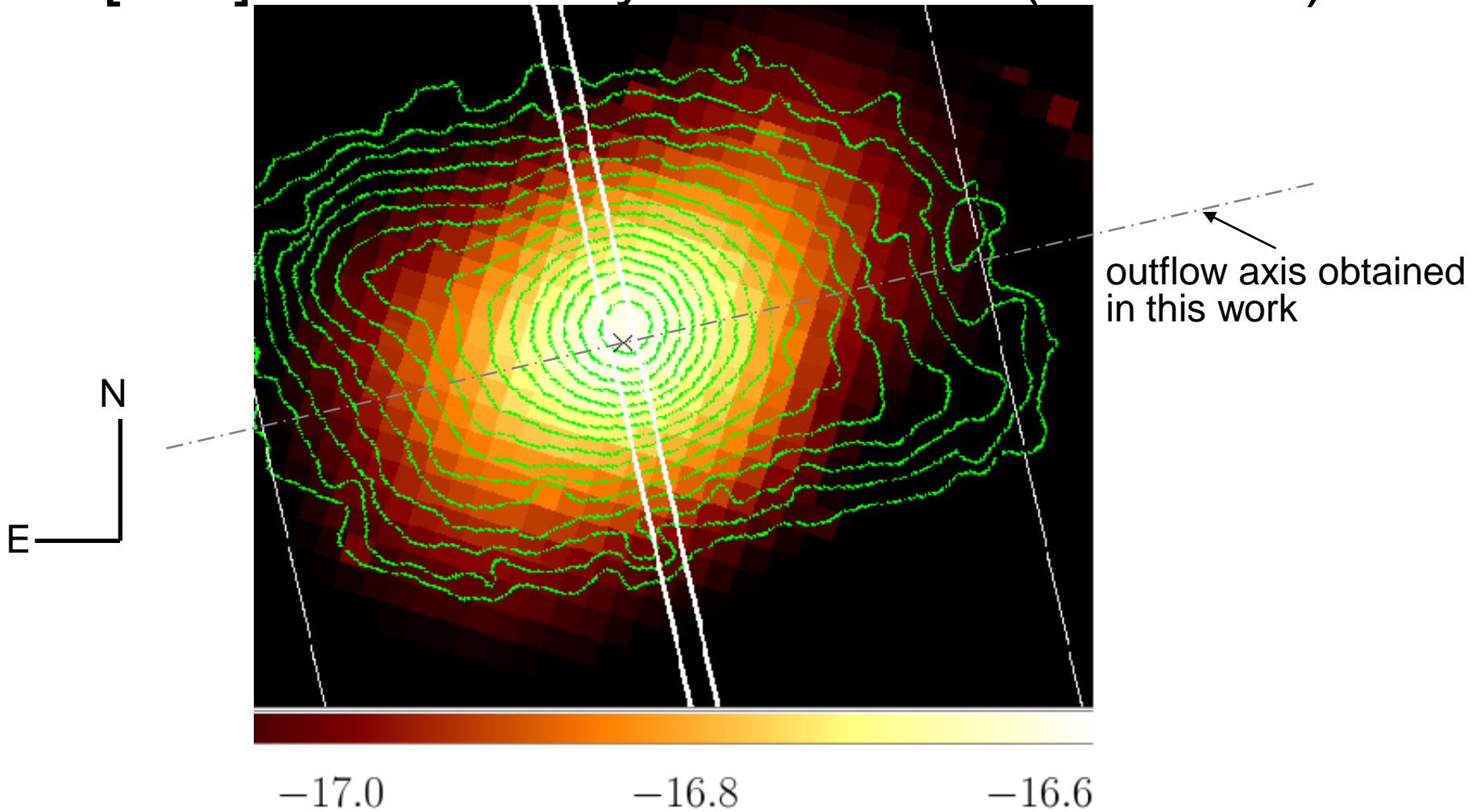


Spectrum of central region of NGC 1052



Spectrum of the central $0''.4 \times 0''.4$ region of NGC 1052. The spectrum of the central region of NGC 821 is also shown, after matching redshift and flux between the two galaxies. The bottom spectrum is the **continuum-subtracted** one of NGC 1052.

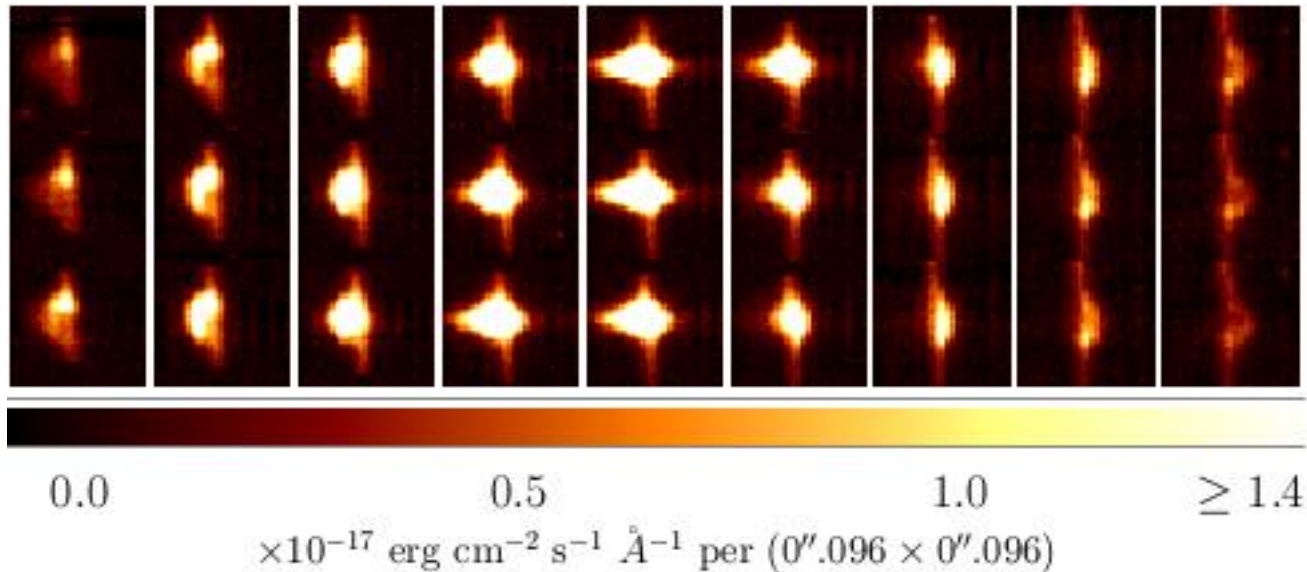
[OIII] line intensity distribution (contours)



Contours: total intensity distribution of [OIII] λ 5007 line in $\log_{10} I$ [I erg cm $^{-2}$ s $^{-1}$ per (0".096 x 0".096)lens]. The contour interval is 0.1 with the lowest contour level -16.27.

Colors: spatial distribution of the averaged line-free continuum in $\log_{10} F$ [F erg cm $^{-2}$ s $^{-1}$ A $^{-1}$ per lens]. X: location of the continuum peak. Thick white lines denote one of "pseudo slits" described in next figure while thin lines show "scanned" region.

Three components



A “pseudo-slit” representation scan through the continuum-subtracted data cube. The position angle of the pseudo slits was set to $\sim 13^\circ$, vertical to the axis of outflow. Only the [OIII] λ 5007 line is shown. The twenty seven panels are for each 0”.096-width pseudo slit, stepped every 0”.096. For each panel, the horizontal axis runs over the wavelength range of 5002.3 Å (left) to 5068.6 Å (right). The vertical axis is spatial: 37 lenses with 0”.096 sampling. NNE is up and SSW is down.

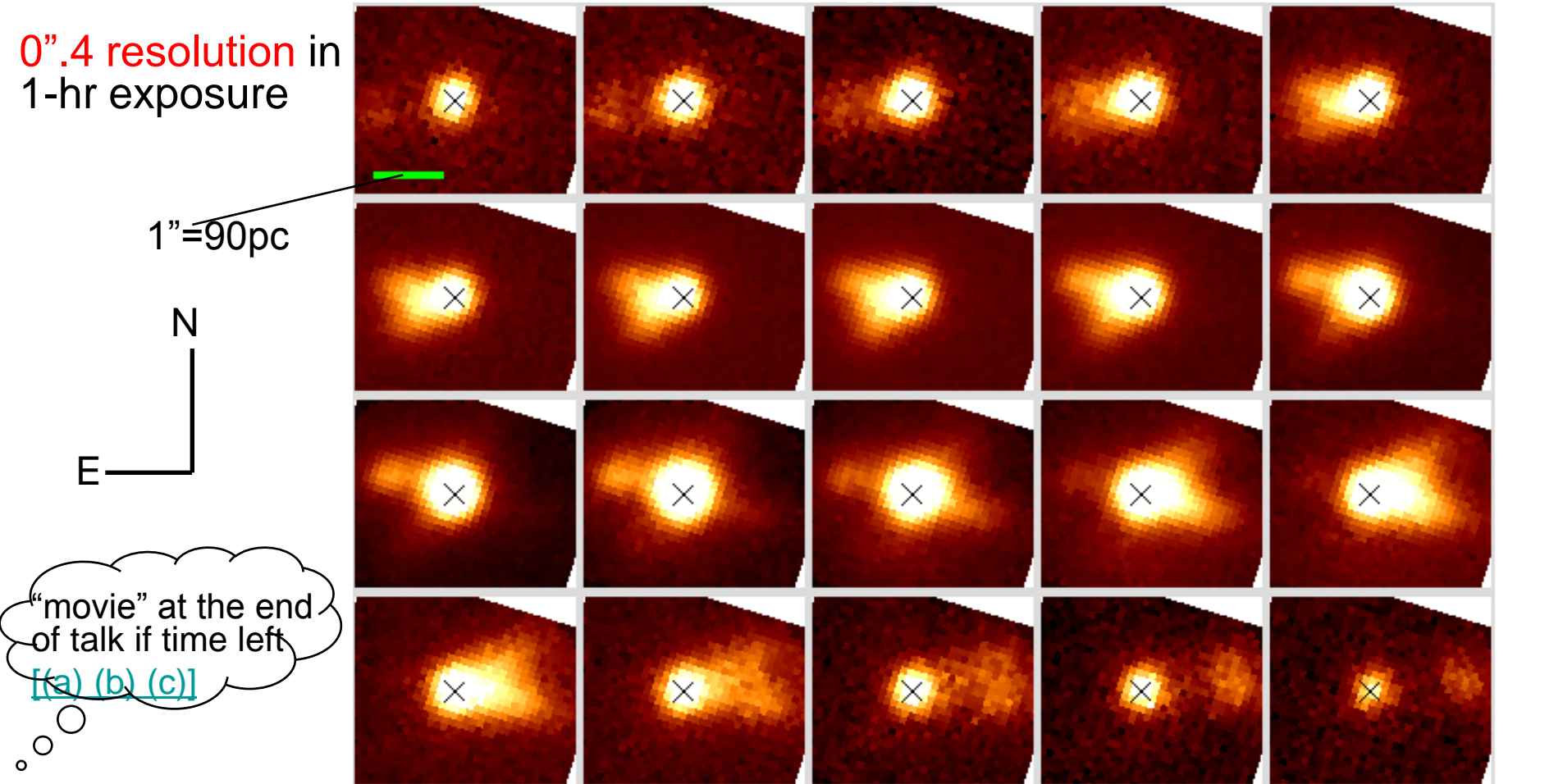
- (1) Narrow component: low-velocity, narrow comp. over the whole region.
- (2) **High-velocity component: within radius $\sim 1''$ from the nucleus.**
- (3) Nuclear component: spatially unresolved in our data.

Structures in bipolar outflow

Figure in next page---Velocity channel maps. Bipolar outflow.

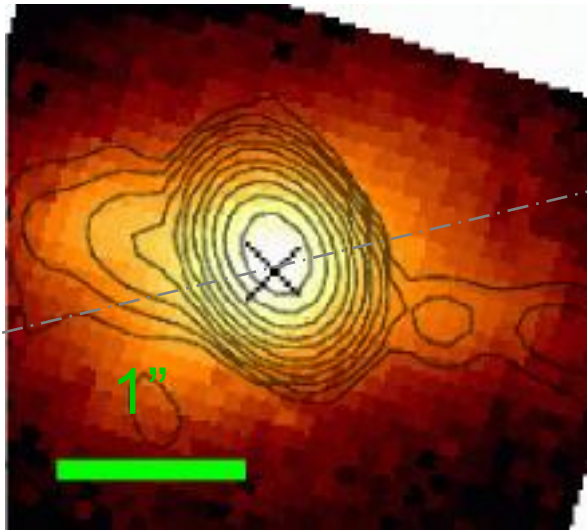
- The opening angle of the outflow decreases with velocity shift from the systemic velocity **both** in bluer and redder velocity channels.
 - explained only if the outflow has **intrinsically higher-velocity components inside, i.e., in regions closer to the outflow axis.**
- At both sides of the bipolar outflow, the highest velocity components are detached from the nucleus.
 - This gap can be explained by an **acceleration** of at least a part of the flow or the surrounding matter, or by **bow shocks** that may be produced by even higher velocity outflow components that are not yet detected.

Velocity channel maps of [OIII] λ 5007 line

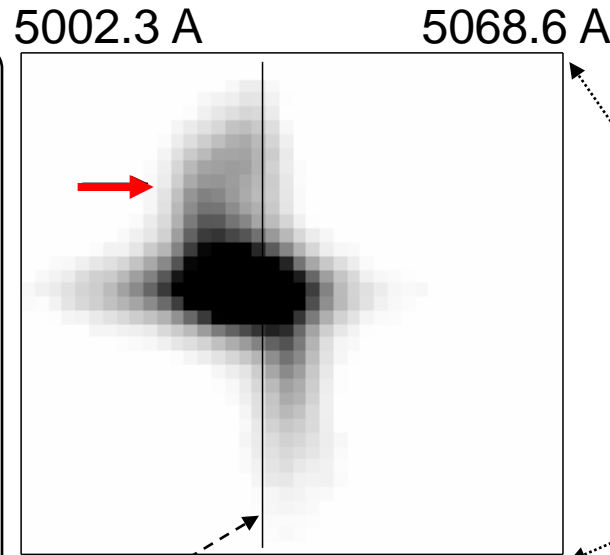


Velocity channel maps of the [OIII] λ 5007 line for every 1.7 Å, which corresponds to 102 km s⁻¹. The wavelength ranges from 5012.5 (top left) to 5044.8 Å (bottom right). The intensity scale among the channels is arbitrary. The cross denotes the location of the line-free continuum peak.

Bipolar outflow & radio jets

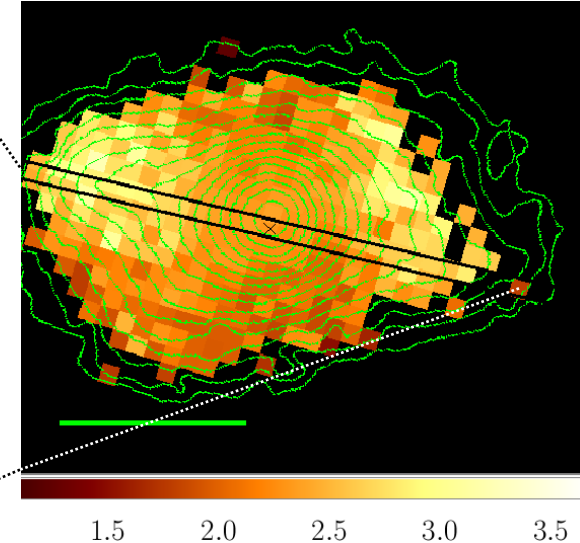


Comparison of $[\text{OIII}]\lambda 5007$ line emission (color) ridges with MERLIN 1.4 GHz contours (Kadler et al. 2004)



systemic velocity

Abrupt change in the velocity field



Spatial distribution of $[\text{OIII}]\lambda 5007/\text{H}\beta$ line ratio (color), with $[\text{OIII}]\lambda 5007$ intensity contours

Strong $[\text{OIII}]$ emission **ridges** along the edges of the outflow.

[left] closely related with the 1"-scale radio jet-counterjet structure.

[middle] abrupt change in the velocity field of the ionized gas.

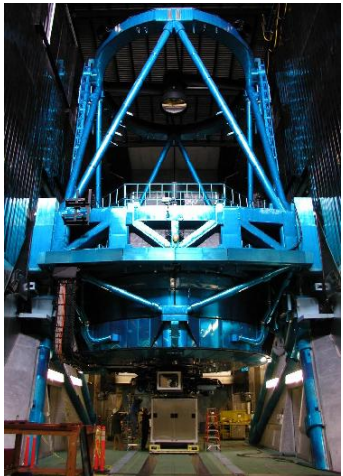
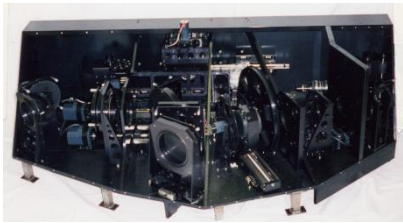
[right] large $[\text{OIII}]/\text{H}\beta$ flux ratio explained by shocks ($\sim 100\text{km s}^{-1}$).

-> **Strong interaction** of the jets (+ some ridge components) with ISM.

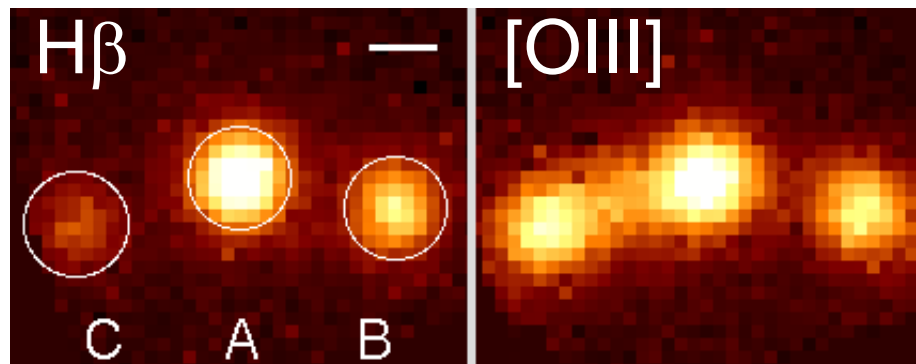
Summary (NGC 1052)

- **High spatial resolution IFS** of “prototypical” LINER NGC 1052
→ Young ($\sim 10^5$ yr) outflow from AGN
- **Structures** in outflow
Intrinsic velocity dependence on angle from outflow axis.
Acceleration?
or Bow shock by unseen high velocity component?
Relation with radio jets.

Integral field spectroscopy of the quadruply lensed quasar 1RXS J1131-1231: new light on lens substructures



1. Macro/milli-lens
2. Microlens
3. Summary



Three “kinds” of gravitational lenses

- Macrolens ($\sim 10^{12} M_{\odot}$)

Smooth potential of the whole lens galaxy.

Determines rough structure, such as lensed image positions.

- Millilens ($\sim 10^8 M_{\odot}$)

CDM clumps expected in the lens galaxy halo.

- Microlens ($\sim 10^0 M_{\odot}$)

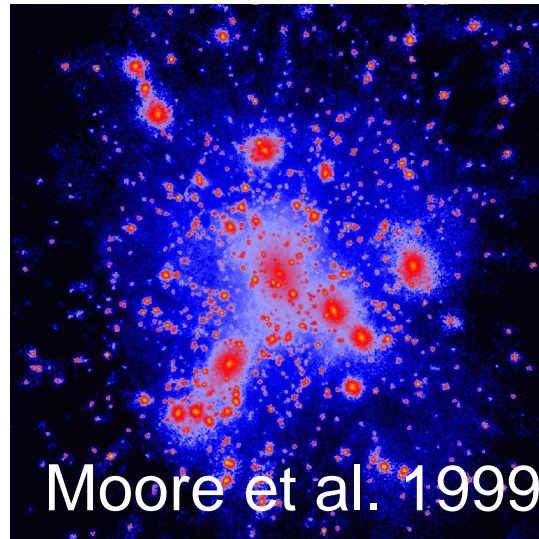
each \sim stellar mass object in the lens galaxy.

Abstract (1RXS J1131-1231)

- Mass of any substructures along the line of sight $M_E < 10^5 M_\odot$
- **Resolving** the structure of quasar **narrow line region** (with macrolensing)
- **Microlenses** for quasar broad line region
For quasar images C & (partially) A.
Resolving broad line region for image A.

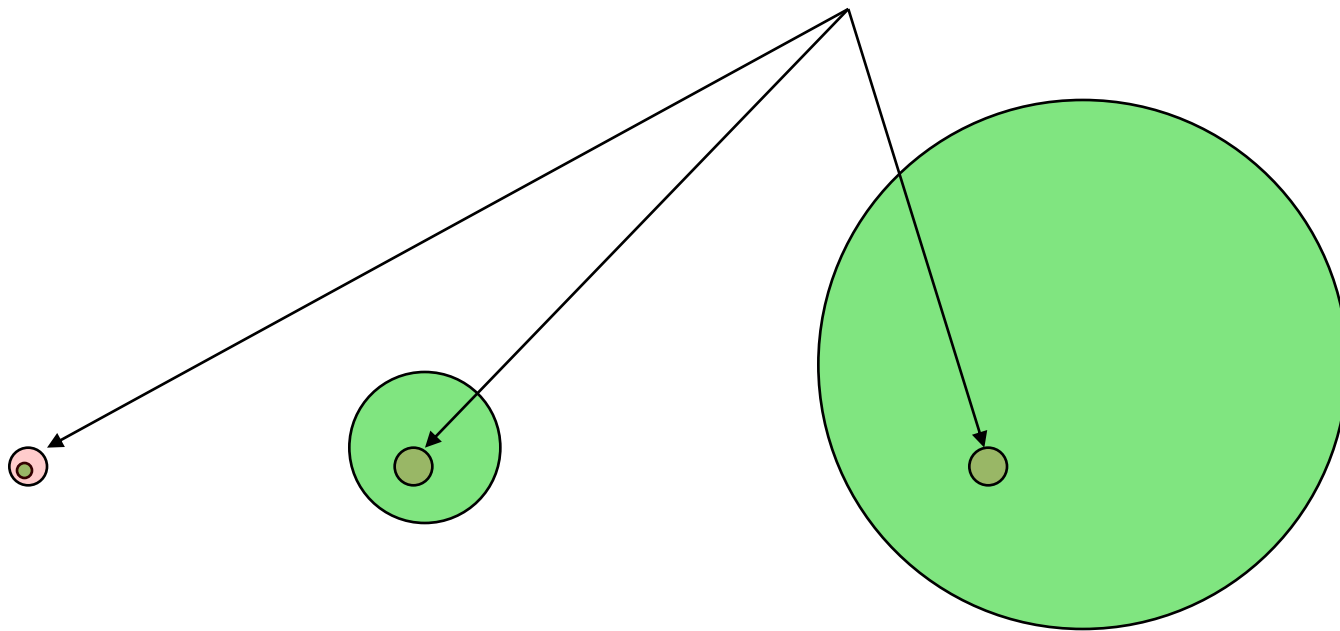
Section 1

(Macro&)Milli-lens



Investigating the existence of **millilens** by using **Narrow line flux ratios** among quasar images

When the **Einstein radius** ($\propto M_E^{1/2}$) is fixed,



lensing effects on green-colored regions are



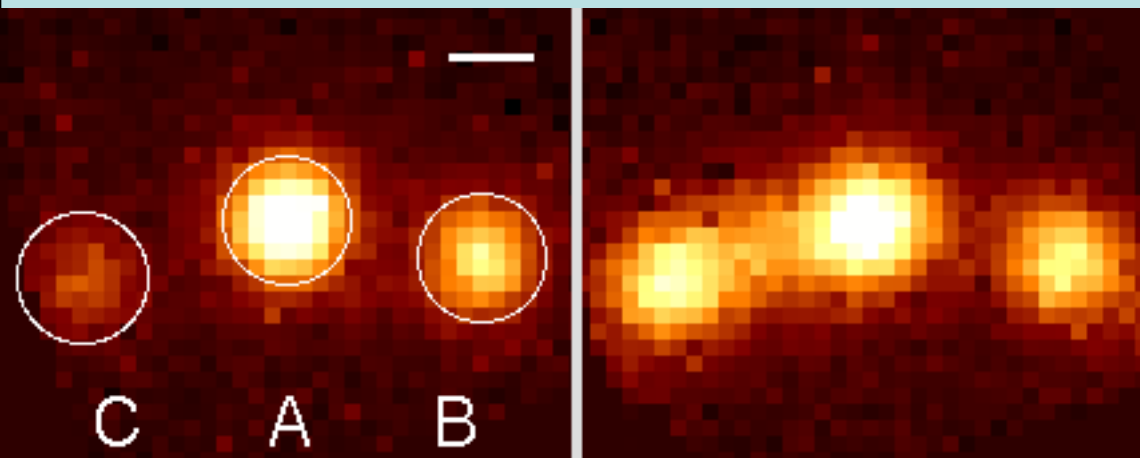
Micro/milli-lens mass & Emission line region size

	Narrow line region 10^2 pc $\sim 1.4 \times 10^{-2}''$	Broad line region $10^{-1} \sim 2 \text{ pc}$ $\sim 1.4 \times 10^{-5} \sim 6''$
This work		
Microlens (star $\sim 1 M_{\odot}$ $\theta_E \sim 2.4 \times 10^{-6}''$)	Not affected	Affected
Millilens (CDM subhalo $\sim 10^8 M_{\odot}$ $\theta_E \sim 2.4 \times 10^{-2}''$)	Affected	Affected

Observations

Kyoto 3DII IFS mode (37x37 lenslet array)
+ Subaru 8.2m telescope

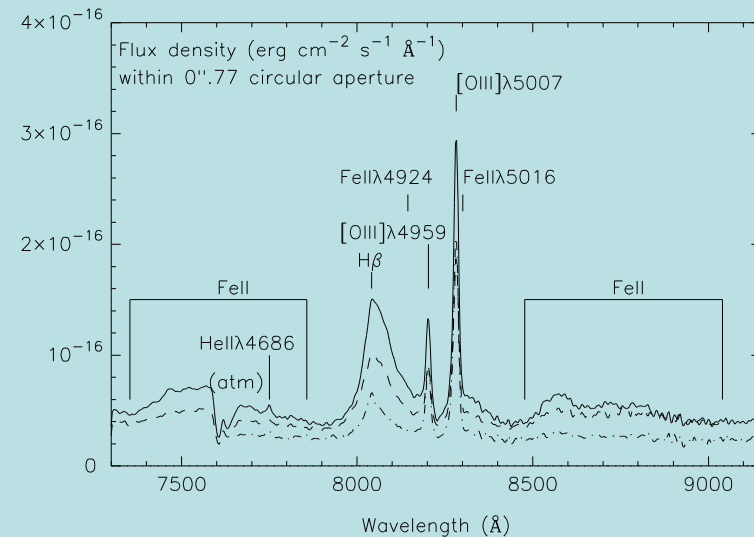
- Spatial sampling = $0''.096 \text{ lenslet}^{-1}$; FOV $\sim 3''.6 \times 2''.8$
- Spatial resolution = $0''.5\text{-}0''.6$



$H\beta$ (broad line)

[OIII](narrow line)

White bar = $0''.5 = 2.2 \text{ kpc}$ at $z_{\text{Lens}}=0.295$. $z_S=0.658$.
The faintest image D is out of FOV.



[OIII] ratios are consistent with macrolens model !

(As for C/B, contribution from extended emission between A & C.)

TABLE 1
RELATIVE FLUX RATIOS AMONG QUASAR IMAGES A, B, AND C

	Line ^a	A	B	C
Obs.	[O III]	1.63 ^{+0.04} _{-0.02}	1.00	1.19 ^{+0.03} _{-0.12}
	H β (broad)	1.74 ^{+0.07} _{-0.12}	1.00	0.46 ^{+0.02} _{-0.03}
Macrolens models	SIEx ^b	1.66	1.00	0.91
	SISx ^c	1.75	1.00	1.00
	SISx ^d	1.70	1.00	0.96

Accurate flux ratio measurements.
image separation $\sim 1''$

Conclusion[1.1] Millilens

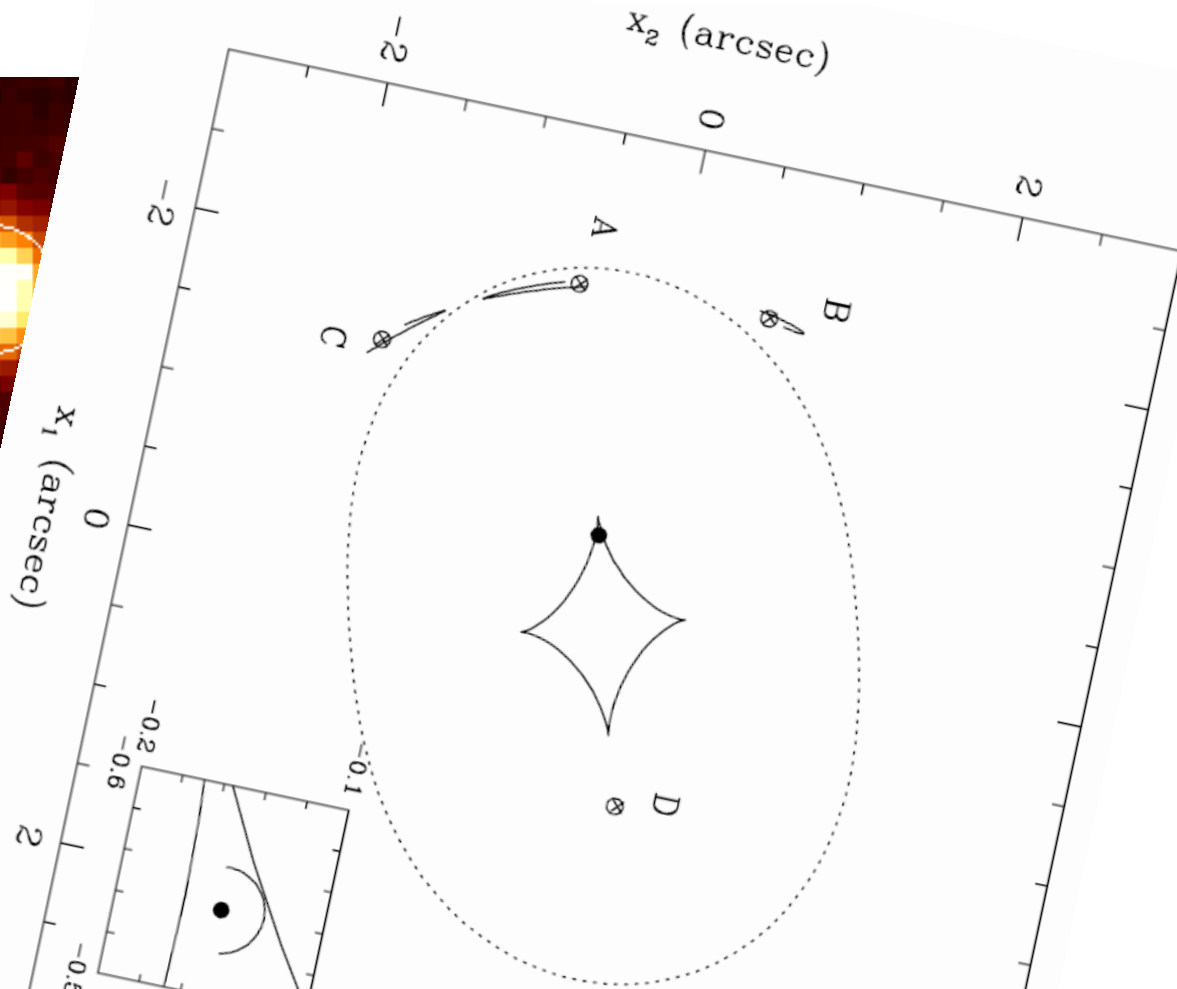
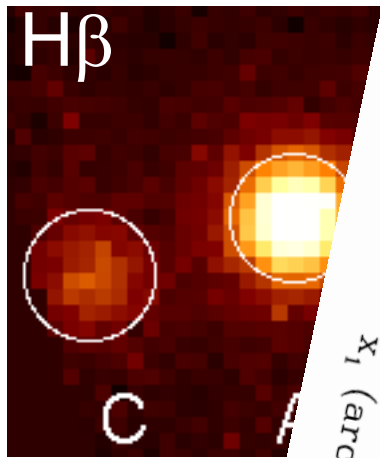
Mass of any substructures
along the line of sight
(quasar images A, B, C)

$$M_E < 10^5 M_\odot$$

Conclusion[1.2] Macrolens

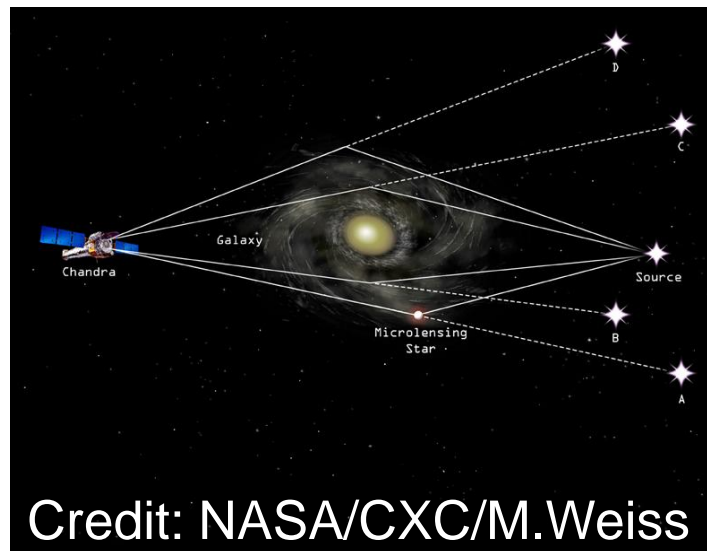
Resolving Structure of Narrow line region(asymmetry)

Without magnification,
 $\sim 100\text{pc} = 14\text{milliarcsec}$



Section 2

Microlens



Credit: NASA/CXC/M.Weiss

$H\beta$: A/B ratio is consistent with macrolens model.
 C/B ratio is inconsistent!
 → Microlens

TABLE 1
 RELATIVE FLUX RATIOS AMONG QUASAR IMAGES A, B, AND C

Line ^a		A	B	C
Obs.	[O III]	$1.63^{+0.04}_{-0.02}$	1.00	$1.19^{+0.03}_{-0.12}$
	$H\beta$ (broad)	$1.74^{+0.07}_{-0.12}$	1.00	$0.46^{+0.02}_{-0.03}$
Macro lens model	SIEx ^b	1.66	1.00	0.91
	SISx ^c	1.75	1.00	1.00
	SISx ^d	1.70	1.00	0.96

Conclusion[2.1] Microlens

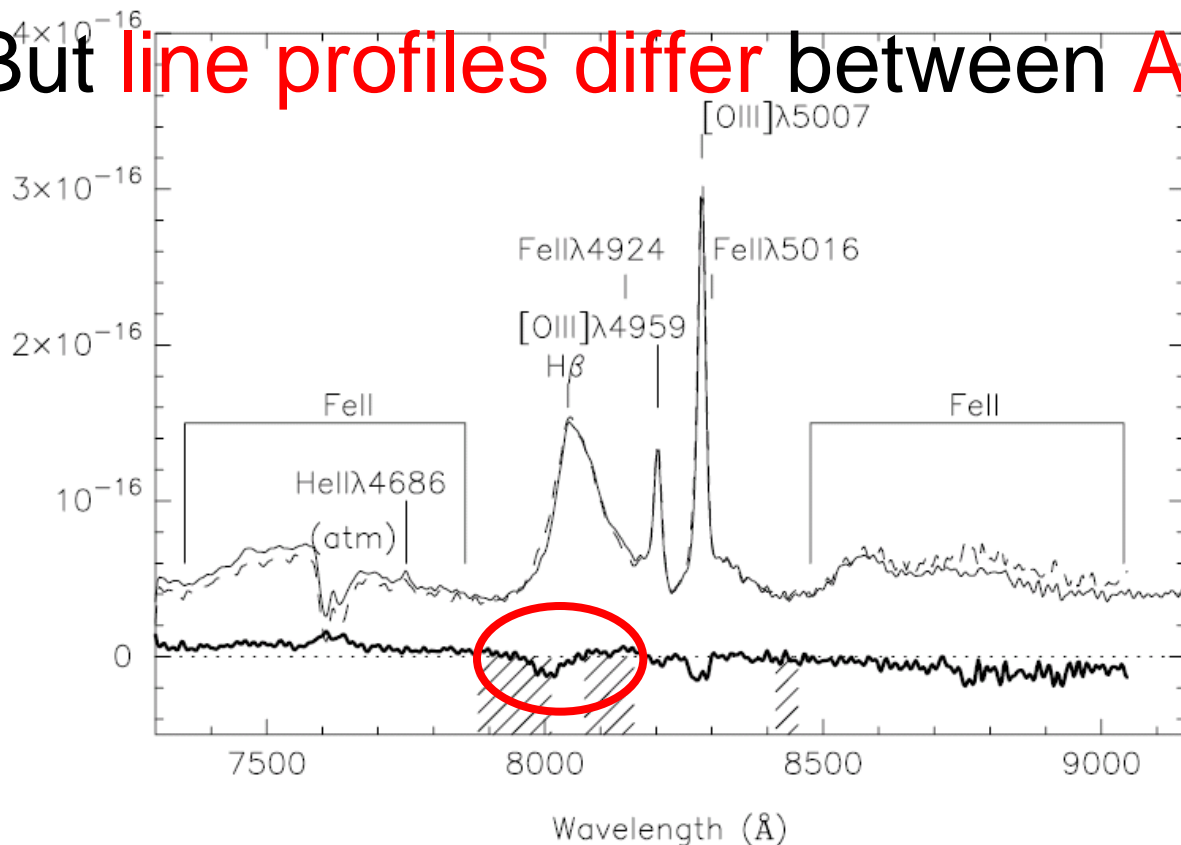
Quasar image **C** is demagnified
by **microlensing**.

Conclusion[2.2] Microlens

“Resolving” structure of broad line region

The A/B ratio of H β (broad line) is consistent with macrolens model.

But **line profiles differ** between A & B.

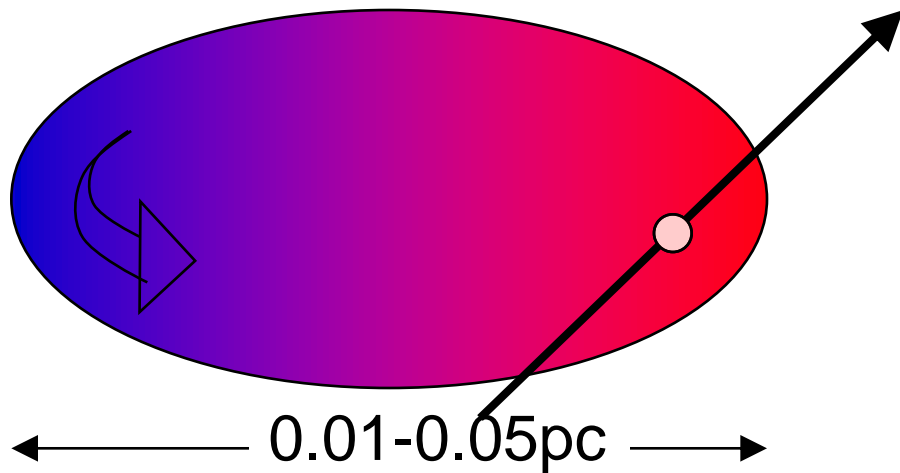


Comparison between image A & 1.74 x image B

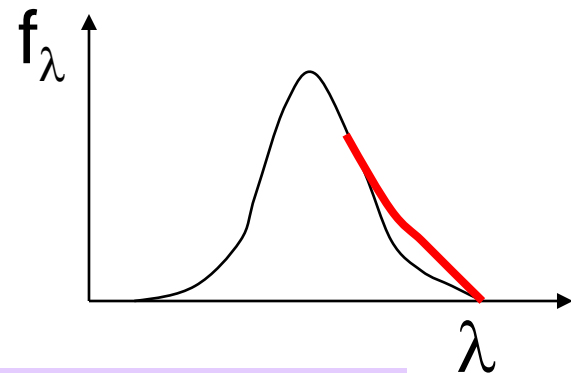
“Resolving” structure of quasar broad line region with microlens

Line profile depends on which part is microlensed.

If gas is rotating,



line profile will change when a microlens passes through.



Better “resolution” than $\sim 1 \mu\text{arcsec}$

Summary (1RXS J1131-1231)

- Mass of any substructures along the line of sight $M_E < 10^5 M_\odot$
- **Resolving** the structure of quasar **narrow line region** (with macrolensing)
- **Microlenses** for quasar broad line region
For quasar images C & (partially) A.
Resolving broad line region for image A.

Summary of this talk

IFS mode of Kyoto 3DII

Optimized for high spatial resolution
with $\sim 0''.1$ sampling

LINER **NGC 1052**

AGN outflow structures

Gravitational lens system **1RXS J1131-1231**

Mass distribution in lens galaxy &

Structure of line emission regions in quasar